earth

Article

Impact of Wind on the Spatio-Temporal Variation in Concentration of Suspended Solids in Tonle Sap Lake, Cambodia

Michitaka Sato [1], Rajendra Khanal [1,2,*], Sovannara Uk [1], Sokly Siev [3,4], Ty Sok [5] and Chihiro Yoshimura [1]

[1] Department of Civil and Environmental Engineering, School of Environment and Society, Tokyo Institute of Technology, 2-12-1-M1-4, Ookayama, Meguro-ku, Tokyo 152-8552, Japan; tokodai88@gmail.com (M.S.); uk.s.ab@m.titech.ac.jp (S.U.); yoshimura.c.aa@m.titech.ac.jp (C.Y.)

[2] Policy Research Institute, A Think-Tank of the Government of Nepal, 3rd Floor of Federal Secretariat Construction and Management Building, Sano Gaucharan-5, Kathmandu 44600, Nepal

[3] General Department of Science, Technology & Innovation, Ministry of Industry, Science, Technology & Innovation, Preah Norodom Boulevard, Sangkat Phsar Thmey III, Khan Daun Penh, Phnom Penh 120203, Cambodia; siev.sokly@misti.gov.kh

[4] Research and Innovation Center, Institute of Technology of Cambodia, Phnom Penh 12000, Cambodia

[5] Faculty of Hydrology and Water Resources Engineering, Institute of Technology of Cambodia, Russian Federation Blvd., P.O. Box 86, Phnom Penh 12156, Cambodia; sokty@itc.edu.kh

* Correspondence: rajendra.khanal@gmail.com

Abstract: Even though wind, water depth, and shear stress are important factors governing sediment resuspension in lakes, their actual relations to total suspended solids (TSS) distribution in natural environments have not been well elucidated. This study aims to elucidate the impact of the wind on the spatio-temporal variation of TSS in Tonle Sap Lake, Cambodia, during low-water (March and June, <1 m) and high-water (September and December, 8–10 m) seasons. To this end, wind and TSS data for December 2016 and March, June, and September 2017 were collected and analyzed. For spatial interpolation of wind speed, the inverse distance weighted method was found to be better ($R^2 = 0.49$) than the vectorized average ($R^2 = 0.30$) and inverse of the ratio of distance ($R^2 = 0.31$). Spatial interpolation showed that the wind speed and direction on the lake were <5 m/s and southward during the low-water season and <7 m/s and westward during the high-water season. The TSS concentration in the low-water season was higher (>50 mg/L) than that in the high-water season. The TSS concentration during the low-water season was empirically described by wind speed (W), water depth (D), and shear stress (τ_wave) with a function of W^3, W^3/D, and $exp^{(W/D)}$ or $exp^{(\tau\_wave)}$, depending on the location in the lake. The critical shear stress due to wind-induced waves at most of the places in the lake was higher than the total shear stress indicated. Sedimentation was predominant in December and June, and erosion (siltation) was dominant in March. Most of the siltation in March was dominant in the southern part of the lake.

Keywords: wind speed and direction; spatio-temporal; total suspended solids; interpolation; shear stress; Tonle Sap Lake

1. Introduction

Sediment re-suspension occurs because of the advection and diffusion of sediments into water columns by wind events when bottom shear stresses are enough to entrain materials from the lake bed [1,2]. Sediment resuspension takes from hours to days to reach equilibrium condition, when total suspended solids (TSS) are uniformly distributed in lakes [3–9]. The basic physical processes and dominant factors in cohesive sediment transport in shallow lakes are flocculation, deposition, siltation, and environmental parameters (e.g., wind speed, water depth, and vegetation type) [1,10,11].

A number of studies that have analyzed the impact of habitat structure, land use land cover, hydrodynamic properties, and sediment and organic matter characteristics on sediment resuspension are available [12–14]. The relationship of wind-induced sediment

resuspension between wind and shear stress based on TSS simulation from force derived by shear stress in the water bottom had been developed using a highly dimensional hydrodynamic model [11,15–18]. However, the spatial distribution of wind-induced re-suspension and simplified empirical equations based on meteorological and environmental factors to elucidate the interaction of the wind with TSS simulations have not been assessed in detail. A pragmatic approach that can describe the relationship of wind waves and total suspended sediment concentrations is to use relatively simple empirical formulas that can utilize wavelength as a function of wind velocity and fetch, and re-suspension occurs if the total shear stress is greater than the critical shear stress, which is considered the case if the wavelength exceeds twice the water depth. The basic processes involved in cohesive sediment transport, such as flocculation, deposition, and erosion, have been studied by many scientists [10].. Carper and Bachmann (1984) [19] and Scheffer (2004) [5] showed that an empirical approach works well to describe re-suspension in a shallow lake. In addition, models based on the nonlinear shallow water equation for coastal engineering have been widely used to quantify wind and several physical wave characteristics, including wave height, length, peak period, maximum orbital velocity, and shear stress [20,21].

Håkanson and Bryhn (2008) [22] reviewed the mechanisms of wave development, which can be calculated on the basis of the bottom current velocity (computed from water depth, wave height, wave length, and wave period). Resuspension occurs when deep-water waves enter water shallower than one-half of the wavelength. The extent of re-suspension is also a function of the energy imparted to the system by wind waves and lake bathymetry. At low wind speed, no resuspension occurs as the critical fetch is larger than the maximum fetch in a lake. Above a critical wind speed, the re-suspended fraction of a lake rises with increasing wind. Due to the sharp decrease in re-suspension with water depth, a change in water level can affect wind-induced re-suspension.

Siev et al. (2018) [23] investigated sediment dynamics in Tonle Sap Lake (TSL) and observed simulated TSS concentration to fit well with the observed TSS concentration during flooding. However, during other periods, such as during dry and wet seasons when water depth and wind speed varies a lot, TSS concentration was underestimated, probably because of the lack of understanding of the influence of wind on the spatio-temporal variation of TSS. The transfer of energy from wind that leads to a variation of TSS concentration is dependent on the spatio-temporal variation of metrological parameters, especially wind speed, and the physical properties of the sediment, such as particle size, shear stress, and time to reach equilibrium [24].

The simultaneous action of wind-induced currents and surface waves leads to an increase in the bottom shear stress, which may exceed the critical shear stress and cause re-suspension [1,25]. The occurrence of shear stress in the water column is divided into two parts, namely, currents and waves. Surface waves have a more pronounced contribution to re-suspended sediments than the currents [11,26–29]. Current-induced shear stress is dominant in open channels and rivers, whereas in lakes and ponds, wave-induced shear stress contributes to sediment resuspension [26,30–32]. In general, wave-induced shear stress contributes as much as 70% of the total re-suspension in shallow lakes [33].

The general objective of this study is to elucidate the impact of the wind on the spatio-temporal variation in concentration of suspended solids in TSL. The specific objectives include (i) finding a proper method for spatial interpolation of the wind and (ii) elucidating the relationship of sediment re-suspension to wind, sediment characteristics, and other environment variables for TSS estimation.

2. Materials and Methods

2.1. Study Area

TSL, one of the largest freshwater lakes with unique reversal hydrodynamics flowing between Mekong River (MR) and Tonle Sap River (TSR), is of utmost importance for economic, livelihood, culture, and recreation not only in Cambodia but also in lower Mekong Basin. There are two distinct seasons in Cambodia, namely, wet and dry. As a

result, TSL has distinct features during the dry and wet seasons. The area, length, width, and depth of TSL vary from 2.5k to 15k km^2, 120 to 250 km, 3 to 100 km, and <1 to as much as 10 m during dry and wet seasons, respectively. The average outflow from TSL to TSR during the dry season and inflow from MR to TSL during the wet season vary from 380 to 8200 m^3/s and from 100 to 7000 m^3/s, respectively. During the wet season, there is a huge influx of sediment discharge from MR to TSL, and in one of the studies, as much as 80% of sediment influx from the Mekong Basin has been found to be retained by TSL [23,34,35]. The TSS concentrations during dry and wet seasons vary from 4 to 650 mg/L and from 3 to 125 mg/L, respectively (reference: TSL fact sheet in [36]). TSL is always under the influence of the wind. The average and maximum wind speeds during dry and wet seasons vary from 3–4 to 6.2–8.8 m/s and from 2–3 to 12.3 m/s, respectively.

Sedimentation across TSL during the dry season varies from 0.1 to 0.16 mm/year [37]. The sedimentation rate during dry and wet seasons varies in the range 306.7 ± 369.6 to 194.4 ± 43.3 g/m^2/day [23]. During the dry season, when the lake is very shallow (<1 m), there is active re-suspension of the sediment in the lake [34]. The sediment of TSL and the floodplain mainly composed of silt (4–63 μm) and clay (<4 μm), which is favorable for re-suspension [23]. The map of the study area, sampling sites for wind speed, and TSS collection cross section (CS) point are shown in Figure 1.
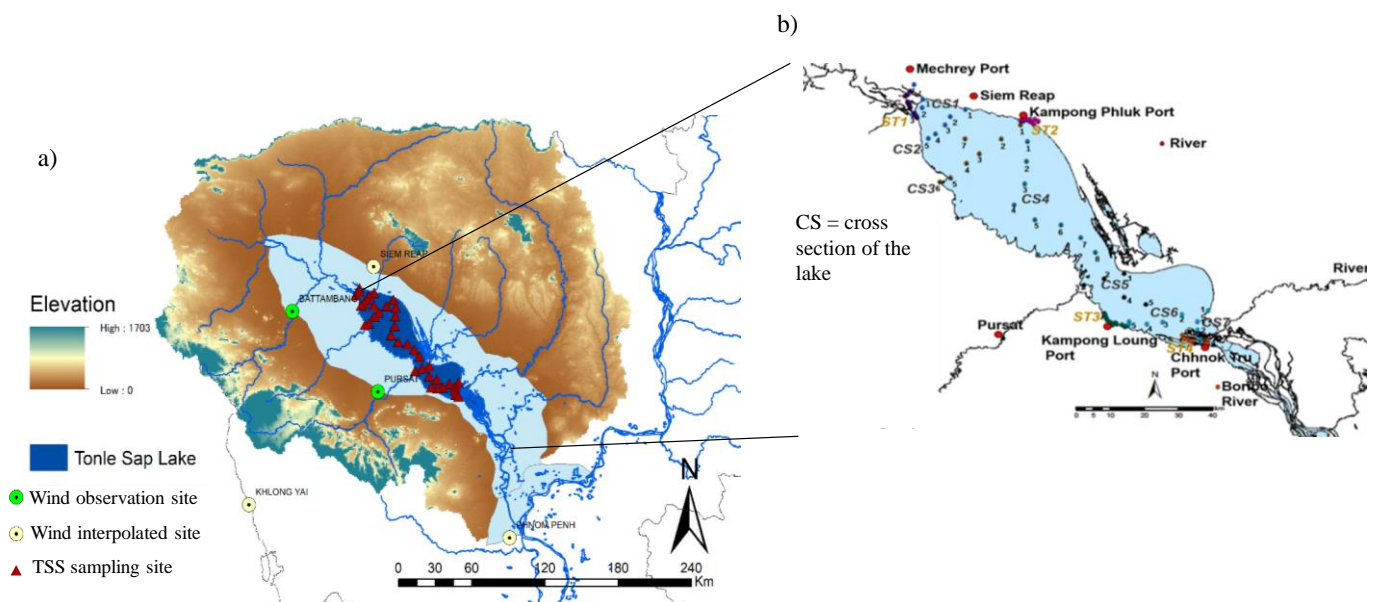

Figure 1. (**a**) Study area and (**b**) cross sections (CS) of Tonle Sap Lake, Cambodia, for the sampling of total suspended solids.

2.2. Data Preparation

Wind data were obtained from the Natural Climatic Data Center from 1949 to 2019 at 12 stations in Cambodia. However, because many wind datapoints were missing and none covered wind across TSL, it was necessary to sort the wind data and to use interpolation to find wind characteristics at a particular location in TSL. Before interpolation, it is a prerequisite to characterize the data. Wind data were interpolated by three methods: (i) inverse distance weighted (IDW) in ArcGIS; (ii) vectorized average; and (iii) inverse of ratio of distance. The interpolated data were selected by best-fit Pearson correlation coefficient (*r*) and root mean square error (RMSE) among those three methods (Table 1). A detail methodology for interpolation is given in Supplementary File S1.

Table 1. Pearson correlation coefficient (*r*) and RMSE of interpolation for wind data.

IDW	Pursat						Battam Bang		Average	
Year	**2008**		**2009**		**2010**		**2010**			
Evaluation Value	*r*	RMSE	*r*	RMSE	*r*	RMSE	*r*	RMSE	*r*	RMSE
(1) Speed										
IDW	0.75	0.68	0.57	0.70	0.31	1.19	0.32	0.70	0.49	0.81
Vectorized average	0.78	1.11	0.36	1.26	0.20	1.96	−0.14	0.84	0.30	1.29
Inverse of ratio	0.55	0.91	0.17	0.98	0.56	1.65	−0.05	0.96	0.31	1.13
(2) Direction										
IDW	−0.35	122	−0.11	162	0.60	255	−0.19	163	−0.01	176
Vectorized average	0.31	56	0.34	176	−0.58	192	−0.12	83	−0.01	127
Inverse of ratio	0.24	142	0.27	145	0.12	284	−0.43	177	0.05	187
(3) Direction + Speed (Inner product)										
r										
IDW	−0.02		−0.28		0.14		0.07		−0.02	−0.02
Vectorized average	0.06		0.05		0.00		−0.24		−0.03	0.06
Inverse of ratio	−0.45		0.07		0.66		−0.40		−0.03	−0.45
(4) Direction + Speed (Polar coordinates)										
r	*x*	*y*	*x*	*y*	*x*	*y*	*x*	*y*	*x*	*y*
IDW	0.32	−0.63	0.25	0.01	−0.55	0.24	0.54	−0.62	0.14	−0.25
Vectorized average	0.64	0.61	0.55	0.40	0.04	−0.30	0.23	0.22	0.36	0.23
Inverse of ratio	0.89	0.33	−0.42	−0.90	0.49	−0.24	0.48	0.37	0.36	−0.11
RMSE	*x*	*y*	*x*	*y*	*x*	*y*	*x*	*y*	*x*	*y*
IDW	1.21	3.38	2.37	3.30	0.57	3.48	1.39	4.02	1.39	3.55
Vectorized average	1.19	1.30	2.92	1.92	0.55	1.05	1.53	1.56	1.55	1.46
Inverse of ratio	1.32	3.11	1.37	2.85	1.32	3.13	0.26	3.80	1.07	3.22

As the speed calculation direction of the wind is also important, vectorized speed should be taken for the average calculation. Wind data were characterized across each CS (CS 1 to 7; Figure 1). Characterization of wind data was conducted using a wind rose diagram, which shows the speed and direction of the wind at a location for a specified time interval. The graphical wind data were then sorted by wind speed and direction such that the distance covered by wind per unit time could be calculated. The wind rose diagrams from December 2016 and March, June, September, and December 2017 at three locations, namely, Khlong Yai, Siem Reap, and Phnom Penh, are shown in Supplementary File S1. Data sorted from the wind rose were then taken for the interpolation of the wind at various locations.

For wind speed, the value of *r* from the IDW method in Pursat for 2008 and 2009 was greater than or equal to 0.57, and for 2010, *r* from the inverse of ratio method was 0.56 (Table 1). Depending on the year and site, the *r* and RMSE values were different. No specific interpolation methods could be said to be the ideal method, but IDW could be said to be comparatively better than the vectorized average and inverse of ratio method as the average *r* from IDW (0.49) was comparatively greater than that from vectorized average (0.30) and inverse of ratio (0.31). However, wind direction should also be considered while interpolating wind speed. Interpolation of wind speed was conducted using two methods, namely, inner product and polar coordinates. In inner product, each value of wind speed and direction was expressed as one vector, and the product of observed and interpolated

wind data was taken as the inner product, the cosine value of which gave the Pearson correlation coefficient. In the polar coordinate method, polar coordinates were obtained by converting from linear coordinates to polar coordinates and by taking the average. The weighted r and RMSE for wind speed and direction from the IDW method can be said to be comparatively better than those from the other two methods, consistent with an earlier finding [38]. Hence, interpolation of wind speed by IDW was applied for TSS simulation.

2.3. TSS and Other Environmental Variables

The TSS data are the same as those reported earlier [23], and were collected during September 2016 to June 2017. Besides TSS, other environmental variables were also analyzed, namely, particle size distribution of suspended sediments, average diameter of sediment particles, settling velocity, air and water temperature, precipitation, and water depth.

The average diameter of sediment particles was calculated by the mass ratio of sediment and settling velocities as governed by Stokes' law as shown in Equation (1):

$$\beta = \frac{D_{s50}^2 (\rho_s - \rho_0) g}{18 \eta},$$ (1)

where β is the settling velocity (m/s), ρ_s, ρ_0 are the densities of the sediment and fluid (g/cm^3), g is gravity acceleration (m/s^2), and η is fluid viscosity (g/cm/s). Settling velocity varied spatially but not temporally.

2.4. Empirical Relationships

Empirical relationships between wind and TSS were derived using observed TSS, interpolated wind speed, and other environmental parameters (i.e., water level and shear stress). The method of derivation is nonlinear regression analysis using the least squares method, and accuracy of the derivation is compared by correlation coefficient under three conditions: (i) the whole area of TSL, (ii) season variation, and (iii) a specific CS in a lake. Empirical analysis is based on the assumption that sediment suspension occurs under steady-state conditions. The details of the empirical calculation are given in Supplementary File S2.

2.5. Mechanism Elucidation of Wind-Induced Sediment Re-Suspension

In order to estimate the balance of the total shear stress (wind-induced waves and currents) and critical shear stress on sediment re-suspension and to analyze the fluctuation of TSS throughout the lake, wind-induced sediment re-suspension was evaluated using two methods: (i) shear stress analysis and (ii) assessment of re-suspension rate. The details of the mathematical calculation of these two methods are given in Supplementary File S3.

Shear stress can be calculated by the following equation:

$$\tau_{wave} = H \times \frac{\rho \left(v_0 \left(\frac{2\pi}{T} \right)^3 \right)^{0.5}}{2 sinh \frac{2\pi D}{L}},$$ (2)

where τ_{wave} is the shear stress by wind-induced waves (Pa), ρ is water density, v_0 is the kinematic viscosity of water (cm^2/s), H is wave height (cm), T is wave period (s), D is water depth (cm), and L is wave length (cm). Wave period and length can be calculated using the different equations of Bretschneider methods [39]. Waves are considered long waves and deep-water waves during dry and wet seasons, respectively.

The magnitudes of bottom shear stresses due to current (τ_{curr}) and wind-induced shear stress at the surface of the lake (τ_0) are estimated using a quadratic drag law, as given in Equation (3):

$$|\tau_{curr}| = 0.1\tau_0 = 0.1 C_D \rho_a W^2,$$ (3)

where ρ_a denotes the density of air and C_D denotes the drag coefficient

$$C_D = 0.001(0.75 + 0.067W). \tag{4}$$

Shear stress due to currents in large shallow lakes such as TSL is significantly smaller than the shear stress due to waves [40]. Hence, it is necessary to balance the critical shear stresses (τ_{cr})

$$\tau_{cr} = \tau_c^* \rho R g D_{s50}, \tag{5}$$

where $R = \rho_s - \rho/\rho$ (the submerged specific gravity), ρ_s is the sediment density, D_{s50} denotes the sediment grain size, and g is the acceleration due to gravity. The critical (nondimensional) Shield's parameter τ_c^* can be obtained by curve fittings to the experimental dataset for incipient motion developed by [41]:

$$\tau_c^* = 0.5 \times \left[0.22 Re_p^{-0.6} + 0.06 \times 10^{(-7.7 Re_{ep}^{-0.6})} \right], \tag{6}$$

where $Re_p = \sqrt{gRD_{s50}}D_{s50}/\eta_0$, with η_0 denoting the kinematic viscosity of water.

Re-suspension rate was calculated by following Equation (7):

$$\frac{dS}{dt} = \frac{1}{D}(-\beta S + E), \tag{7}$$

where S is the depth-averaged suspended sediment concentration $\left(\text{mgm}^{-3}\right)$, D is the depth of the water column (m), β is the settling velocity $\left(\text{ms}^{-1}\right)$, and E is the erosion rate $\left(\text{mgm}^{-3}\text{s}^{-1}\right)$. Additionally,

$$E = \alpha W^p, \tag{8}$$

where α and p are empirical constants and W is the wind speed $\left(\frac{m}{s}\right)$.

Putting the value of **E** in Equation (8) and differentiating yield the value of **S** as given in Equation (9) under steady-state conditions and Equation (10) under unsteady-state conditions.

$$\frac{dS}{dt} = \frac{1}{D}(-\beta S + \alpha W^p), S = \frac{\alpha W^p}{\beta} + \left(S(0) - \frac{\alpha W^p}{\beta} \right) e^{-(\beta t/D)}, \tag{9}$$

$$\frac{dS}{dt} = f_0 exp\left(-\frac{U}{PE}\right) = f_0 exp\left(K\frac{H^a}{D} \times W^b\right), \\ S = f_0 exp\left(K\frac{H^a}{D} \times W^b\right)t + S(0). \tag{10}$$

In addition, to understand re-suspension dynamics, it is required to identify the time required to reach equilibrium TSS. This equilibrium time was compared for three months December, March, and June. In addition, convergence of TSS $\left(= \frac{\alpha W^p}{\beta}\right)$ was considered the maximum TSS and background TSS $(= S(0))$ was considered the minimum TSS in the whole TSL and in each point (CS1–CS7). The monthly average settling velocity (β) and water depth (D) were used for the calculation of suspended sediment concentration (S).

3. Results and Discussion

3.1. Characterization of Wind Data

The comparison of the wind speed and direction observed at Khlong Yai, Siem Reap, and Phnom Penh from December 2016 to December 2017 is shown in Figure 2 and Table 1. In March, the wind direction is mainly southward and changes toward the southeast or southwest depending on the locations (see the wind rose diagram in Supplementary File S1 and Table 2). The difference in wind speed is probably due to difference in altitude. Khlong Yai is at a lower altitude of 6 m compared to Siem Reap at 8 m and Phnom Penh at 12 m. The wind speed in December and March was, in general, less than 5 m/s, but in June and September, the wind speed was as much 7 m/s (Table 2).

3.2. Interpolation of Wind Data

The interpolated wind speeds at various CS across TSL and observed TSS are shown in Figure 3. The TSS concentration, in general, during the wet season in December and September was less than 50 mg/L, but during the dry season in March and June, it was greater than 50 mg/L and peaked up to 400 mg/L in March and was greater than 600 mg/L in June (Figure 3). The difference in TSS concentration can be explained by the difference in sediment characteristics, namely, sediment diameter, sediment ratio, and settling velocity, as shown in Table 3. Sand, silt, and clay did not differ much across various CS. However, settling velocity differed because of the difference in the average diameter of sediment particles. For example, the settling velocities at CS3-5 and CS7-3 were higher (>10 m/day) and the average particle diameter was higher (>10 μm) than at other points. The larger the sediment size, the faster the settling velocity and the lower the TSS concentration. The average sediment diameter at CS4 was smaller than that in other CSs. Hence, the settling velocity at CS4, in general, was smaller and the TSS concentration was higher than that in other CSs (Table 3). It can be concluded that one of the factors that influence TSS concentration is the particle size or the settling velocity. In addition, because TSS did not exhibit direct correlation with the wind speed (Figure 3), it was felt necessary to identify the empirical relation of TSS with the wind by adding additional factors such as shear stress and water depth.
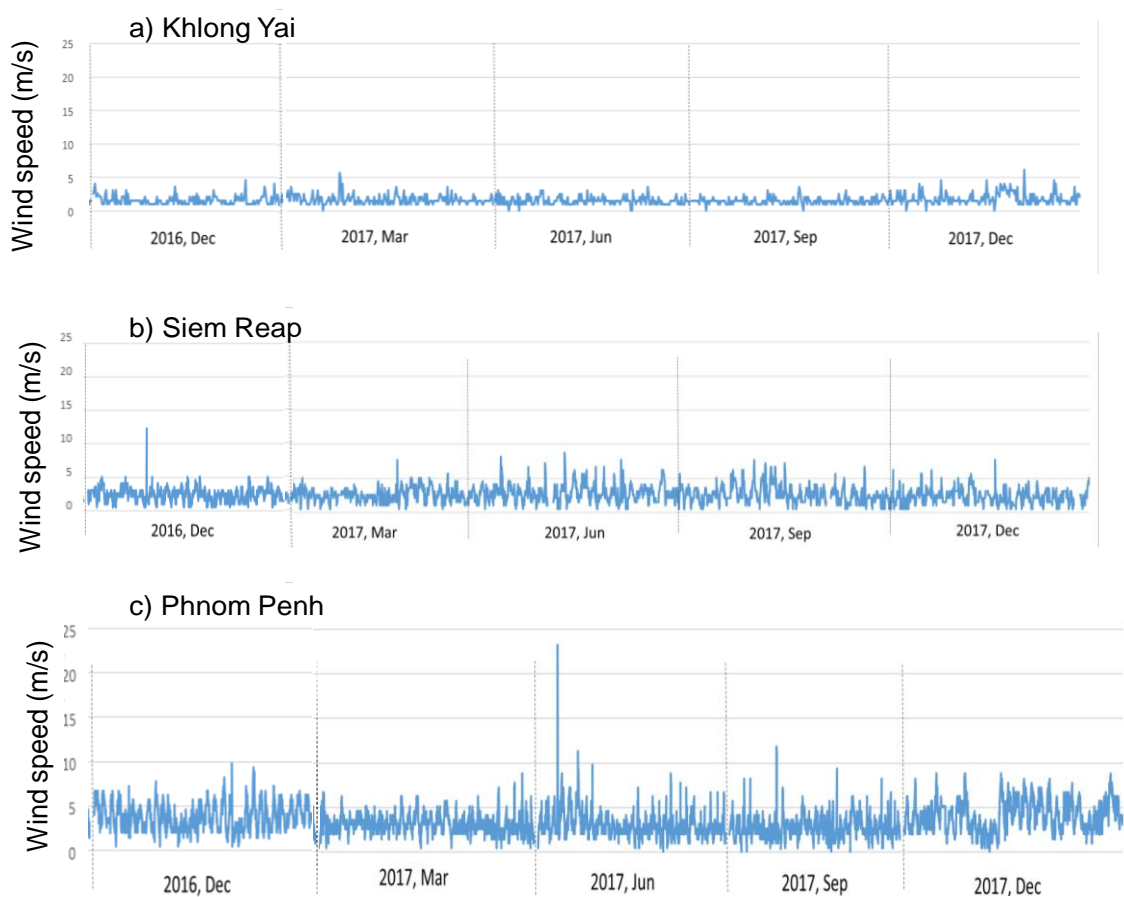
Figure 2. Wind speed in Cambodia at (**a**) Khlong Yai, (**b**) Siem Reap, and (**c**) Phnom Penh.

Month	Wind		Total Suspended Solid (TSS)
	Wind Direction	Wind Speed	
	(1) Khlong Yai (2) Siem Reap (3) Phnom Penh	(1) Khlong Yai (2) Siem Reap (3) Phnom Penh	
December	Direction changes to N at once 1: Trends change slightly between 2016 and 2017, but mainly is westward 2,3: Direction changes to N at once	1: Higher in 2017 than in 2016, and similar in range as in Mar 2: Max: 12.3 m/s, turbulence calms down compared to Sep 3: Average increases compared to Sep	• TSS varies by year • Compared to 5–12.5 mg/L in 2016, TSS are higher than 50 mg/L • CS4-1 only is over 200 mg/L
March	Trends do not change regardless of year 1: Main direction: West or East wind, No NE or SW direction 2: Frequent southern wind, relatively unstable 3: Only SE in 2016 and 2017	1: Relatively lower wind speed (Ave: 3–4 m/s, max: 3.6–5.7 m/s) 2: Occasional stronger wind (7.2–8.2 m/s) 3: Max: 6.2–8.8 m/s	• Completely different wind speed on each location • Higher TSS (>200 mg/L) in: CS2-2, CS3-2, CS3-7, CS4-1~4–3, CS6-2~6–5 • Ave: 169.5, max: 405, min: 4.5 (mg/L) • Strong wind ≠ High TSS • Shallow depth ≠ High TSS
June	Trends do not change regardless of year 1: NS from EW in Mar 2: SW stable 3: SW to SE in Mar	1: Average does not change in Mar, max changes (3.6 m/s in Mar → 15.4 m/s in Jun) 2: Increases by 5 m/s from 7.2–8.2 → 8.8–13.3 m/s 3: Speed does not change, with occasional max, 6.2–8.8 → 12.9–23.2 m/s	• Highest TSS Max: 652 mg/L • CS2 and CS3 have higher TSS • Some places showed lower TSS than that in Mar
September	Trends do not change regardless of year 1: Frequent westward, 2016 and 2017 show same trends. 2: Overall westward, NW ratio increases in 2017 3: S and N from SW 4: Westward wind trend remainsDirection varies by year	1: No turbulence and a stable wind of 2–3 m/s 2: 15–20 m/s in 2016, no turbulence and a stable wind around 7 m/s 3: Speed is the same or slightly higher than that in Jun at around 10 m/s	• Max: ~50 mg/L • Strong wind ≠ High TSS • Relatively stable and lower TSS
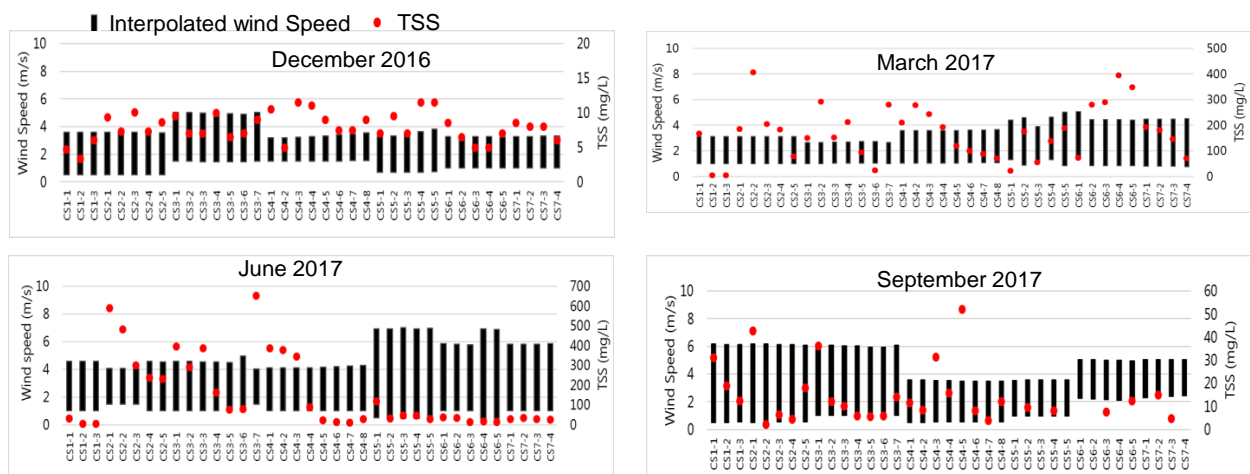
Figure 3. Interpolated wind speed and total suspended solids (TSS) concentration across Tonle Sap Lake, Cambodia.

Table 3. Sediment characteristics across various cross sections (CS) in Tonle Sap Lake, Cambodia.

Area	Point	Average Diameter (μm)	Settling Velocity (m/day)	Mass Ratio of Sediment (%, Sand, Silt, Clay)
CS1	CS1-1	6.50	4.16	
	CS1-2	6.48	4.14	
	CS1-3	5.08	2.55	
CS2	CS2-1	6.78	4.53	
	CS2-2	4.86	2.33	
	CS2-3	5.50	2.98	
	CS2-4	5.61	3.11	
	CS2-5	7.84	6.05	
CS3	CS3-1	6.87	4.65	
	CS3-2	5.48	2.96	
	CS3-3	5.65	3.15	
	CS3-4	3.42	1.16	
	CS3-5	10.9	11.7	
	CS3-6	9.36	8.65	
	CS3-7	4.46	1.96	
CS4	CS4-1	2.49	0.61	
	CS4-2	6.28	3.89	
	CS4-3	2.28	0.51	
	CS4-4	2.62	0.68	
	CS4-5	3.00	0.89	
	CS4-6	6.48	4.14	
	CS4-7	5.83	3.35	
	CS4-8	2.71	0.72	

Table 3. *Cont.*

Area	Point	Average Diameter (μm)	Settling Velocity (m/day)	Mass Ratio of Sediment (%, Sand, Silt, Clay)
CS5	CS5-1	5.85	3.37	
	CS5-2	4.80	2.27	
	CS5-3	8.01	6.33	
	CS5-4	1.68	0.28	
	CS5-5	2.02	0.40	
CS6	CS6-1	7.38	5.37	
	CS6-2	4.19	1.73	
	CS6-3	2.15	0.46	
	CS6-4	3.94	1.53	
	CS6-5	3.10	0.95	
CS7	CS7-1	7.83	6.05	
	CS7-2	3.49	1.20	
	CS7-3	10.3	10.4	
	CS7-4	3.31	1.08	

3.3. Empirical Relation

A number of empirical relations were tried for the correlation of TSS with wind speed, water depth, and shear stress (Supplementary File S3), and they can be summarized as a best-fit curve for the whole lake, dry and wet seasons, and various CS as shown in Table 4.

It is evident from Table 4 that a single equation does not fit well to the simulated TSS across the whole TSL (R^2 = 0.06) or even during dry (R^2 = 0.06) and wet seasons (R^2 = 0.03). As the TSL lake is huge and its area and depth vary from <1 m and 5 km^2 to 5 m and 16 km^2 during the dry and wet seasons, respectively, it is necessary to segregate the lake based on cross sections and to propose an empirical relation for each CS, and during each season.

The correlation coefficient increased from CS1 to CS7 while moving from the northern to the southern part of the lake, and TSS was better correlated by squared or cubed transformation of wind speed over water depth and power exponent of wind speed (Table 4), which was in agreement with the hypothesis that the higher the wind speed is, the higher is the TSS. In general, the most significant empirical equations for various CS were the following: CS1 = $exp(W/D)$; CS2 = W^2 or W^3/D; CS3, CS4, and CS5 = W^3 or W^3/D; CS6 = W^3 or $exp(W)$; and CS7 = W^3/D (Figure 4).

Table 4. Empirical relation for TSS in Tonle Sap Lake, Cambodia.

	Regression Relation	R^2	RMSE
Whole lake (dry + wet season)	$TSS = -20.9W^3/D + 102.8W^2/D - 96.1W/D + 75$	0.06	111
Wet season	$TSS = -0.456\tau_{wave} + 8$	0.03	2.0
	$TSS = 0.80W^3 - 3.9W^2 + 4.5W + 8$	0.02	2.0
Dry season	$TSS = 459.3W^2 - 2244.5W + 2861$	0.06	141
Dry season			
Cross section 1	$TSS = 5.6 \times 10^{-5} \times exp(5W/D) + 5$	0.96	53
Cross section 2	$TSS = -3766.9W^2 + 19242W - 23467$	0.71	259
	$TSS = -143.6W^3/D + 146W^2/D + 132.7W/D + 540$	0.69	256
Cross section 3	$TSS = -310.3W^3 + 1331.3W^2 - 702.7W - 1399$	0.42	198
	$TSS = -1232.4W^3/D + 6050W^2/D - 7417W/D + 368$	0.41	182
Cross section 4	$TSS = 723.0W^3 - 2757W^2 + 1128.8W + 3156$	0.59	159
	$TSS = 2731.3W^3/D - 12498.2W^2/D + 14129.7W/D + 72$	0.59	156
Cross section 5	$TSS = 128.3W^3/D - 617.4W^2/D + 750.8W/D + 22$	0.56	79
	$TSS = -50.9\tau_{wave} + 320$	0.58	73
Cross section 6	$TSS = 437.4W^3 - 1610.5W^2 + 636.1W + 1690$	0.82	175
	$TSS = 1.8 \times 10^{-5} \times exp(6.1W) - 6$	0.81	153
Cross section 7	$TSS = 84.2W^3/D - 165.6W^2/D - 144.2W/D + 53$	0.88	82
	$TSS = 1675.8 \times exp(-0.40\tau_{wave}) - 134$	0.77	51

W = wind speed (m/s), D = water depth (m), τ_{wave} = shear stess (Pa), and TSS = total suspended solids (mg/L).
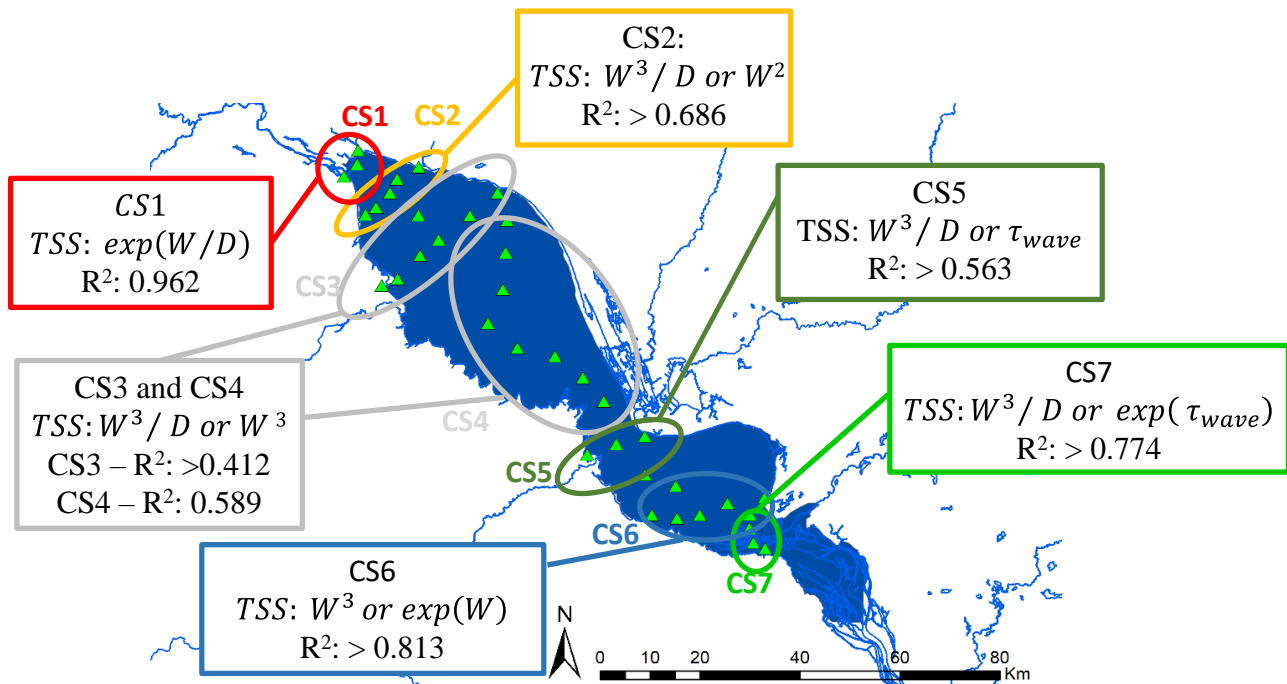

Figure 4. Empirical relation of TSS with the wind speed and lake depth across various cross sections (CS) in Tonle Sap Lake, Cambodia (W = wind speed, D = water depth, and τ_{wave} = shear stress; for details, please refer to Table 4).

The TSS concentration across TSL could be better correlated with wind speed, depth, and shear stress with equations as given in Table 4. As the TSS in the dry season was higher than that in the wet season, the TSS is expected to be affected by wind speed, depth, and shear stress. Even though shear stress is a main factor governing sediment re-suspension, wind speed and depth, but not shear stress, were the primary factors governing TSS concentration (Table 4). For better simulation of TSS concentration, other sediment (settling velocity, wind flux, and wind wave energy) and environmental factors (wave length and wave height) need to be considered in hydrodynamic models.

*3.4. Mechanism of Sediment Re-Suspension*

The current study was conducted to assess the role of the wind field on sediment re-suspension and the probability of sediment suspension using the wind fetch model. On the other hand, the spatial distribution of wind-induced sediment re-suspension has not been thoroughly described and it is necessary to research for sediment re-suspension predictions in large shallow lakes. The impact of water level fluctuation on the sediment dynamics in TSL has been described in a recently published paper [42]. Wave action and subsequent fetches are more likely to cause re-suspension by bottom scouring and are determined by wind speed and fetch [43]. The total shear stress (Pa) as a sum of wind-induced waves and wind-induced currents, and critical shear stress for CS from 1 to 7, for different time periods, December, March, and June, are shown in Supplementary File S3. Critical shear stress at most of the places was higher than the total shear stress (Supplementary File S3), indicating three important points: (i) there was sedimentation (no erosion) of the sediment at most of the CS during the transition period of reversal flow from TSL to MR via TSR in December (end of the rainy season) and from MR to TSL in June (beginning of the rainy season); (ii) most of the sediment that was discharged at various CS in TSL is retained (i.e., no outflow) within the lake; and (iii) whatever erosion of the sediment occurred in TSL, it was predominant in the southern part of the lake at CS5, 6, and 7. Wind-induced wave shear stress was larger than the wind-induced current shear stress, though the latter was negligible. It can be presumed that shear stress could not be said to be the cause of sediment re-suspension as the total shear stress was mostly lesser than the critical shear stress.

The shear stress due to wind-induced waves did not vary at different CS of the lake. In general, the shear stress due to waves is smaller at the center of the lake than at the shore. Shear stress increased toward the shoreline of the lake, perhaps due to transfer of wind energy at the shoreline, as when wind moves from land to middle of the lake, wind energy is much smaller at the middle of the lake where there is much water. This phenomenon could explain why the turbidity at the bank is higher than that at the center of the lake. The higher turbidity at the bank is caused by the shallow water and wave breaking. In this case, it is believed that wind energy is one of the crucial factors governing sediment resuspension, as the energy from the wind near the shoreline is naturally stored and is utilized for sediment re-suspension.

The selected sites, where the total shear stress was greater than the critical shear stress, were then taken for the comparison of shear stress with TSS (Table 5). As shown in Table 5 and Figure 5, TSS decreases with the increase in water depth ($R^2 = 0.57$). Considering that most of the time when the total shear stress was greater than the critical shear stress was in March, which is the middle of the dry season, it can be generalized that the shallower the water depth is, the higher is the total shear stress. The total shear stress increased toward the southern part of TSL. Sediment re-suspension occurred in all seasons in CS7-4, which is located at the southernmost point. Around the south side of TSL, the MR, one of the largest tributaries of TSL, is located nearby, and the inflow of water and sediment from this river has a higher value than that of other tributaries. It can be inferred that sediment re-suspension is likely to occur in places with higher amounts of sediment.

Table 5. Comparison of TSS, water depth, total shear stress, and critical shear stress across selected sites.

Date	Point	TSS (mg/L)	Water Depth (m)	Total Shear Stress (Pa)	Critical Shear Stress (Pa)
21 December 2016	CS7-4	6	8.0	2.93	1.63
30 March 2017	CS5-2	158	0.3	5.85	2.36
15 March 2017	CS5-4	55	0.5	3.30	3.94
16 March 2017	CS5-4	137	1.6	2.53	0.83
26 March 2017	CS5-5	140	0.6	2.26	0.83
15 March 2017	CS6-2	189	1.3	3.06	2.06
15 March 2017	CS6-5	72	0.8	1.76	1.52
15 March 2017	CS7-1	279	0.5	5.81	3.85
15 March 2017	CS7-4	289	1.0	3.25	1.63
2 July 2017	CS7-4	25	5.5	2.66	1.63

$$y = 21.742x^{-0.661}$$
$$R^2 = 0.5691$$
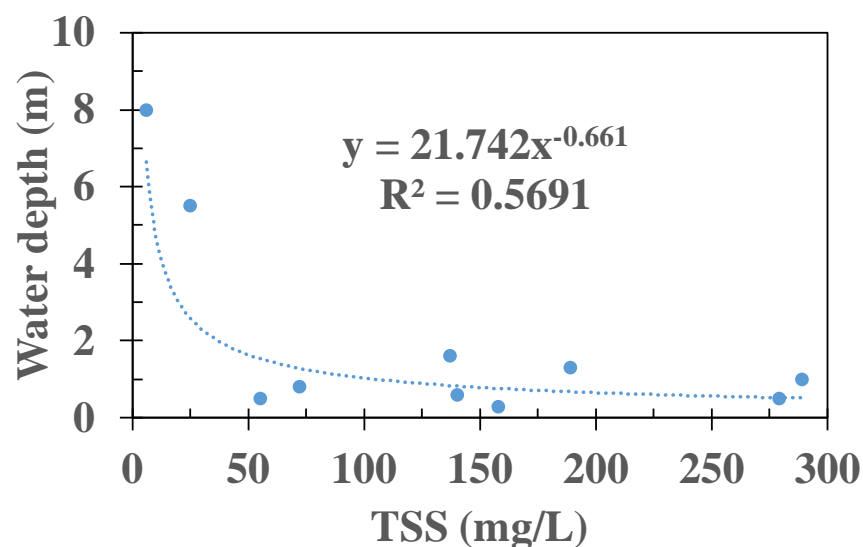
Figure 5. Relationship of TSS with water depth (data source Table 5).

In addition, there was spatio-temporal variation in the relationship between TSS and each environmental parameter (Supplementary File S4). In general, there was a negative correlation among TSS, settling velocity, and critical shear stress. In other words, the lower the settling velocity was, the lower the critical shear stress and the higher the TSS. Loss on ignition (LOI at 550 °C) was higher during the dry season compared to that during the wet season, which meant that the amount of organic matter changed according to season and that it varied greatly depending on the location. As TSL is huge, it is recommended to perform clustering of the lake according to the site for detailed characterization of the TSS and to understand the impact of the wind on sediment re-suspension.

3.5. Time to Reach Equilibrium TSS

The time to reach equilibrium TSS in March, June, and December is shown in Table 6. There was a significant difference in time to reach equilibrium TSS: 9, 20, and 32 days in March, June, and December, respectively, corresponding to average depths of 1.2, 2.7, and 4.7 m (Table 6). The higher the depth is, the higher is the time to reach equilibrium TSS. In addition, time for equilibrium differed, and there were no significant differences in settling

velocity and wind speed in each month. It can be interpreted that there is an impact of the wind and other sediment and environmental factors in governing sediment re-suspension.

Table 6. Calculation of time to reach equilibrium TSS in Tonle Sap Lake, Cambodia.

		March (2017)	June (2017)	December (2016)
Observed TSS (mg/L)	Max $\left(\frac{\alpha W^p}{\beta}\right)$	433	684	15.5
	Min $(S(0))$	4.5	12	4.3
	Ave	176.8	157.4	4.8
Average wind speed (m/s) (W)		2.3	2.5	2.4
Average water depth (m) (D)		1.2	2.8	4.7
Average settling velocity (m/day) (β)		3.2	3.3	3.3
Time for equilibrium TSS (day)		9	20	32

The parameters in Table 6 are based on Equation (11):

$$S = \frac{\alpha W^p}{\beta} + \left(S(0) - \frac{\alpha W^p}{\beta}\right)e^{-(\beta t/D)}, \tag{11}$$

where $\left(= \frac{\alpha W^p}{\beta}\right)$ is considered the maximum TSS and background TSS $(= S(0))$ is considered the minimum TSS in the whole TSL and in each point (CS1–CS7). The monthly average settling velocity (β) and water depth (D) were used for the calculation of suspended sediment concentration (S).

4. Conclusions

- In March, the wind direction is mainly southward and changes toward the southeast or southwest depending on the locations. In general, the wind speed in December and March was less than 5 m/s, but in June and September, the wind speed was as much 7 m/s.
- On the basis of the weighted Pearson correlation coefficient (r) and RMSE, wind interpolation using the IDW method was found to be comparatively better than the vectorized average and inverse of the ratio of distance.
- The TSS concentration, in general, during the wet season in December and September was less than 50 mg/L, but during the dry season in March and June, it was greater than 50 mg/L and peaked up to 400 mg/L in March and greater than 600 mg/L in June. The sediment characteristics with respect to sand, silt, and clay did not differ much across various CS in TSL.
- Settling velocity (m/day) across 37 sites across TSL varied from 0.28 to 11.70, with an average of 3.25 ± 2.75.
- TSS did not exhibit direct correlation with the settling velocity and sediment characteristics (LOI and particle diameter). The empirical equation to correlate TSS with wind speed (W), water depth (D), and shear stress (τ_wave), especially during dry season for different CS across TSL is, CS1= $exp^{(W/D)}$; CS2= W^2 or W^3/D; CS3, and CS4 = W^3 or W^3/D; CS5 = W^3/D or τ_wave; CS6 = W^3 or $exp^{(W)}$; and CS7 = W^3/D or $exp^{(\tau\_wave)}$ (for detailed equation, please refer to Table 4).
- The shear stress due to waves was smaller at the center of the lake and increased toward the shoreline, which is one of the reasons why TSL exhibits higher TSS at the shoreline than at the center of the lake. The total shear stress was greater than the critical shear stress, especially during the dry season in March, when TSS is higher and water depth is lower, compared to the wet season, when TSS is low and water depth is higher.
- The higher wind-induced critical shear stress than the total shear stress at most of the CS in TSL indicated sedimentation occurs predominantly during the transition phase

of the reversal flow between TSL and MR during December and June, and erosion (siltation) is dominant during March. Additionally, most of the siltation in March was dominant in the southern part of the lake, at CS5, 6, and 7.

- The times to reach equilibrium TSS in March, June, and December were 9, 20, and 32 days, respectively. In general, the higher the depth is, the longer the time to reach equilibrium TSS.

References

1. Hawley, N.; Lesht, B. Sediment resuspension in Lake St. Clair. *Limnol. Oceanogr.* **1992**, *37*, 1720–1737. [CrossRef]
2. Vlag, D.P. A model for predicting waves and suspended silt concentration in a shallow lake. *Hydrobiologia* **1992**, *235*, 119–131. [CrossRef]
3. Barica, J. Extreme fluctuations in water quality of eutrophic fish kill lakes: Effect of sediment mixing. *Water Res.* **1974**, *8*, 881–888. [CrossRef]
4. Hamilton, D.P.; Mitchell, S.F. An empirical model for sediment resuspension in shallow lakes. *Hydrobiologia* **1996**, *317*, 209–220. [CrossRef]
5. Scheffer, M. *Ecology of Shallow Lakes*; Springer: Berlin, Germany, 2004; Volume 22.
6. Reddy, K.R.; Fisher, M.M.; Ivanoff, D. Resuspension and diffusive flux of nitrogen and phosphorus in a hyper-eutrophic lake. *J. Environ. Qual.* **1996**, *25*, 363–371. [CrossRef]
7. Søndergaard, M.; Kristensen, P.; Jeppesen, E. Phosphorus release from resuspended sediment in the shallow and wind-exposed Lake Arresø, Denmark. *Hydrobiologia* **1992**, *228*, 91–99. [CrossRef]
8. Ogilvie, B.G.; Mitchell, S.F. Does sediment resuspension have persistent effects on phytoplankton? Experimental studies in three shallow lakes. *Freshw. Biol.* **1998**, *40*, 51–63. [CrossRef]
9. Jalil, A.; Li, Y.; Zhang, K.; Gao, X.; Wang, W.; Khan, H.O.S.; Pan, B.; Ali, S.; Acharya, K. Wind-induced hydrodynamic changes impact on sediment resuspension for large, shallow Lake Taihu, China. *Int. J. Sediment Res.* **2019**, *34*, 205–215. [CrossRef]
10. Chao, X.; Jia, Y.; Shields, F.D., Jr.; Wang, S.S.; Cooper, C.M. Three-dimensional numerical modeling of cohesive sediment transport and wind wave impact in a shallow oxbow lake. *Adv. Water Resour.* **2008**, *31*, 1004–1014. [CrossRef]
11. Luettich, R.A., Jr.; Harleman, D.R.; Somlyody, L. Dynamic behavior of suspended sediment concentrations in a shallow lake perturbed by episodic wind events. *Limnol. Oceanogr.* **1990**, *35*, 1050–1067. [CrossRef]
12. Horppila, J.; Nurminen, L. Effects of submerged macrophytes on sediment resuspension and internal phosphorus loading in Lake Hiidenvesi (Southern Finland). *Water Res.* **2003**, *37*, 4468–4474. [CrossRef]
13. Matisoff, G.; Watson, S.B.; Guo, J.; Duewiger, A.; Steely, R. Sediment and nutrient distribution and resuspension in Lake Winnipeg. *Sci. Total Environ.* **2017**, *575*, 173–186. [CrossRef]

14. Qin, B.; Zhu, G.; Zhang, L.; Luo, L.; Gao, G.; Gu, B. Estimation of internal nutrient release in large shallow Lake Taihu, China. *Sci. China Ser. D* **2006**, *49*, 38–50. [CrossRef]

15. Bailey, M.C.; Hamilton, D.P. Wind induced sediment resuspension: A lake-wide model. *Ecol. Model.* **1997**, *99*, 217–228. [CrossRef]

16. Morales-Marin, L.A.; French, J.R.; Burningham, H.; Battarbee, R.W. Three-dimensional hydrodynamic and sediment transport modeling to test the sediment focusing hypothesis in upland lakes. *Limnol. Oceanogr.* **2018**, *63*, S156–S176. [CrossRef]

17. Bengtsson, L.; Hellström, T. Wild-induced resuspension in a small shallow lake. *Hydrobiologia* **1992**, *241*, 163–172. [CrossRef]

18. Wu, T.; Timo, H.; Qin, B.; Zhu, G.; Janne, R.; Yan, W. In-situ erosion of cohesive sediment in a large shallow lake experiencing long-term decline in wind speed. *J. Hydrol.* **2016**, *539*, 254–264. [CrossRef]

19. Carper, G.L.; Bachmann, R.W. Wind resuspension of sediments in a prairie lake. *Can. J. Fish. Aquat. Sci.* **1984**, *41*, 1763–1767. [CrossRef]

20. Brocchini, M.; Dodd, N. Nonlinear shallow water equation modeling for coastal engineering. *J. Waterw. Port Coast. Ocean Eng.* **2008**, *134*, 104–120. [CrossRef]

21. Rohweder, J.J.; Rogala, J.T.; Johnson, B.L.; Anderson, D.; Clark, S.; Chamberlin, F.; Runyon, K. Application of wind fetch and wave models for habitat rehabilitation and enhancement projects. *Geol. Surv.* **2008**, *1200*, 43.

22. Håkanson, L.; Bryhn, A.C. A dynamic mass-balance model for phosphorus in lakes with a focus on criteria for applicability and boundary conditions. *Water Air Soil Pollut.* **2007**, *187*, 119–147. [CrossRef]

23. Siev, S.; Yang, H.; Sok, T.; Uk, S.; Song, L.; Kodikara, D.; Oeurng, C.; Hul, S.; Yoshimura, C. Sediment dynamics in a large shallow lake characterized by seasonal flood pulse in Southeast Asia. *Sci. Total Environ.* **2018**, *631*, 597–607. [CrossRef]

24. Reeks, M.W.; Reed, J.R.; Hall, D.R. On the resuspension of small particles by a turbulent flow. *J. Phys. D Appl. Phys.* **1988**, *21*, 574–589. [CrossRef]

25. Churchill, J.H.; Williams, A.J.; Ralph, E.A. Bottom stress generation and sediment transport over the shelf and slope off of Lake Superior's Keweenaw peninsula. *J. Geophys. Res. Ocean.* **2004**, *109*, 10.1029/2003JC001997. [CrossRef]

26. Chung, E.G.; Bombardelli, F.A.; Schladow, S.G. Sediment resuspension in a shallow lake. *Water Resour. Res.* **2009**, *45*. [CrossRef]

27. Hawley, N.; Lesht, B.M.; Schwab, D.J. A comparison of observed and modeled surface waves in southern Lake Michigan and the implications for models of sediment resuspension. *J. Geophys. Res. Space Phys.* **2004**, *109*. [CrossRef]

28. Zhang, S.; Nielsen, P.; Perrochet, P.; Jia, Y. Multiscale superposition and decomposition of field-measured suspended sediment concentrations: Implications for extending 1DV models to coastal oceans with advected fine sediments. *J. Geophys. Res. Ocean.* **2021**, *126*, e2020JC016474. [CrossRef]

29. Zhang, S.; Wu, J.; Jia, Y.; Wang, Y.-G.; Zhang, Y.; Duan, Q. A temporal LASSO regression model for the emergency forecasting of the suspended sediment concentrations in coastal oceans: Accuracy and interpretability. *Eng. Appl. Artif. Intell.* **2021**, *100*, 104206. [CrossRef]

30. Ji, Z.-G.; Jin, K.-R. Impacts of wind waves on sediment transport in a large, shallow lake. *Lakes Reserv. Res. Manag.* **2014**, *19*, 118–129. [CrossRef]

31. Reardon, K.E.; Bombardelli, F.A.; Moreno-Casas, P.A.; Rueda, F.J.; Schladow, S.G. Wind-driven nearshore sediment resuspension in a deep lake during winter. *Water Resour. Res.* **2014**, *50*, 8826–8844. [CrossRef]

32. Miao, Q.; Yang, D.; Yang, H.; Li, Z. Establishing a rainfall threshold for flash flood warnings in China's mountainous areas based on a distributed hydrological model. *J. Hydrol.* **2016**, *541*, 371–386. [CrossRef]

33. Sheng, Y.P.; Lick, W. The transport and resuspension of sediments in a shallow lake. *J. Geophys. Res. Space Phys.* **1979**, *84*, 1809–1826. [CrossRef]

34. Kummu, M.; Penny, D.; Sarkkula, J.; Koponen, J. Sediment: Curse or blessing for Tonle Sap Lake? *AMBIO J. Hum. Environ.* **2008**, *37*, 158–163. [CrossRef]

35. Koehnken, L. *IKMP Discharge and Sediment Monitoring Program Review, Recommendations and Data Analysis—Part 2: Data Analysis and Preliminary Results*; Mekong River Commission (MRC): Phnom Penh, Cambodia, 2012.

36. Shivakoti, B.R.; Ngoc-Bao, P. *Environmental Changes in Tonle Sap Lake and Its Floodplain: Status and Policy Recommendations*; Institute for Global Environmental Strategies (IGES): Kanagawa, Japan; Tokyo Institute of Technology (Tokyo Tech): Tokyo, Japan; Institute of Technology of Cambodia (ITC): Phnom Penh, Cambodia, 2020.

37. Tsukawaki, S. Lithological features of cored sediments from the northern part of Lake Tonle Sap, Cambodia. In Proceedings of the International Conference on Stratigraphy and Tectonic Evolution of Southeast Asia and the South Pacific, Bangkok, Thailand, 19–24 August 1997; pp. 232–239.

38. Ali, S.M.; Mahdi, A.S.; Shaban, A.H. Wind speed estimation for Iraq using several spatial interpolation methods. *Environ. Prot.* **2012**, *1*, 2.

39. Bretschneider, F.; De Weille, J.R. *Introduction to Electrophysiological Methods and Instrumentation*; Elsevier: Amsterdam, The Netherlands, 2006.

40. James, W.F.; Barko, J.W.; Butler, M.G. Shear stress and sediment resuspension in relation to submersed macrophyte biomass. *Hydrobiologia* **2004**, *515*, 181–191. [CrossRef]

41. Parker, G.; Toro-Escobar, C.M.; Ramey, M.; Beck, S. Effect of floodwater extraction on mountain stream morphology. *J. Hydraul. Eng.* **2003**, *129*, 885–895. [CrossRef]

42. Khanal, R.; Uk, S.; Kodikara, D.; Siev, S.; Yoshimura, C. Impact of water level fluctuation on sediment and phosphorous dynamics in Tonle Sap Lake, Cambodia. *Water Air Soil Pollut.* **2021**, *232*, 1–15. [CrossRef]

43. Gloor, M.; Wüest, A.; Münnich, M. Benthic boundary mixing and resuspension induced by internal seiches. *Hydrobiologia* **1994**, *284*, 59–68. [CrossRef]